Rev. LatinAm. Metal. Mat.

Artículo Regular

www.rlmm.org

ULTRASONIC PULSE VELOCITY FOR MONITORING THE SUSCEPTIBILITY OF CONCRETE TO SODIUM SULPHATE AND WETTING-DRYING CYCLES

Ricardo A. Cruz H[1], Luis E. Zapata O[1], Luz A. Quintero O[2], Julián O. Herrera[2].*

1: Universidad Industrial de Santander, Facultad de Ingenierías Físico-Mecánicas, Escuela de Ingeniería Civil, Bucaramanga, Colombia. Profesor(es) Escuela de Ingeniería Civil. 2: Universidad Industrial de Santander, Facultad de Ingenierías Físico-Químicas, Escuela de Ingeniería Metalúrgica y Ciencia de Materiales, Bucaramanga, Colombia. Profesor(es) Escuela de Ingeniería Metalúrgica y Ciencia de Materiales.

**e-mail: racruz@uis.edu.co*

ABSTRACT

The external sulphate attack of concrete is related to the formation of expansive sulphate-containing compounds in the hardened state of the concrete samples. The aim of this research is to study the use of the technique of ultrasonic pulse velocity (UPV) to estimate the mechanical and physical changes during an accelerated attack of sodium sulphate combined with wetting-drying cycles. Each cycle consisted in wetting, drying in oven and cooling. This combination tries to replicate field conditions for concrete samples in sulphate-rich environments under climatic changes (wetting/drying). The experimental program consisted of visual inspection, development of cooling curves, X-ray diffraction analysis, UPV measurements, mass and volume changes as well as compressive strength of concrete specimens. Standard concrete cylinders of 100 x 200 mm were used and the accelerated attack was monitored each 15 cycles with a total of 120 cycles. The results showed that both density (physical) and compressive strength (mechanical) measurements agreed with the UPV behavior registered through the external sulphate attack. In addition, mathematical models relating the compression analysis and the density values with the UPV measures were constructed. Finally, the X-ray diffraction results were successfully correlated with the developed mathematical models.

Key words: sulphate attack, concrete, compressive strength, ultrasonic pulse velocity.

VELOCIDAD DE PULSO ULTRASÓNICO PARA MONITOREO DE LA SUSCEPTIBILIDAD DEL CONCRETO A SULFATO DE SODIO Y CICLOS DE HUMECTACIÓN Y SECADO

RESUMEN

El ataque externo de sulfatos en el concreto está relacionado con la formación de componentes que contienen sulfatos expansivos en el estado endurecido de las muestras de concreto. El objetivo de la presente investigación consiste en estudiar el uso de la técnica de la velocidad de pulso ultrasónico (UPV) para estimar los cambios físicos y mecánicos ocurridos durante el ataque acelerado de sulfato de sodio en conjunto con ciclos de humectación y secado. Cada ciclo consistió en humectación, secado al horno y enfriamiento. Esta combinación trató de simular un típico ambiente rico en sulfatos y sometido a cambios climáticos (humectación/secado). El programa experimental consistió de inspección visual, desarrollo de curvas de enfriamiento, análisis de difracción de rayos X, medidas usando UPV, cambios de masa y de volumen y resistencia a la compresión de las muestras de concreto. En la investigación se usaron cilindros estándar de concreto de 100 x 200 mm y el ataque acelerado fue monitoreado cada 15 ciclos con un total de 120 ciclos. Los resultados mostraron que las medidas tanto de densidad (prueba física) como de resistencia a la compresión (prueba mecánica) fueron efectivamente capturadas por el comportamiento de UPV a lo largo del ataque externo de sulfatos. En adición, se construyeron modelos matemáticos que relacionaron las medidas de densidad y de compresión con los resultados de UPV. Finalmente, los análisis de difracción de rayos X fueron satisfactoriamente correlacionados con los modelos matemáticos desarrollados.

Palabras clave: ataque por sulfato, concreto, resistencia a la compresión, velocidad de pulso ultrasónico.

Recibido: 05-03-2015 ; **Revisado:** 08-09-2015

Aceptado: 23-11-2015 ; **Publicado:** 20-02-2016

DOI: *10.5281/zenodo.10031568*

pISSN: 0255-6952 | eISSN: 2244-7113

Rev. LatinAm. Metal. Mat. 2016; **36** (2): 155-167

1. INTRODUCTION

External sulphate attack on concrete structures has been a key durability issue and a subject of extensive investigation. Sulphate attack is defined as a deleterious action involving sulphate ions. Nevertheless, nowadays external sulphate attack is not completely understood [1]. For example, according to Hehdi *et al*. [2] field experience shows that concrete exposed to sulfates can suffer from surface scaling above ground level due to physical attack. This damage has often been ignored and confused with chemical sulfate attack. Therefore, they studied concrete partially-immersed in sulfate solutions and exposed to cyclic temperature and relative humidity. Results show that concrete can experience dual sulfate attack. The lower immersed portion can suffer from chemical sulfate attack, while the upper portion can be vulnerable to physical attack. According to Liu *et al*. [3] chemical sulfate attack is considered a complex physicochemical process that consists in formation of harmful products such as: ettringite, gypsum and thaumasite via chemical reactions with physical crystal growth of these products. On the other hand, physical sulfate attack, also called sulfate salt crystallization or sulfate weathering, refers to the crystallization of sulfates in the pores of concrete without chemical reactions. The mechanism is called physical salt attack because chemical reactions between concrete and crystallizing salt are not involved [4]. In the context of the present document, the word "*attack*" is understood as an action that has resulted in deterioration or in a loss of durability to the concrete. Also, in the present paper there will not be distinction between chemical or physical sulphate attacks. It is important to clarify because the mere fact of a given chemical reaction involving sulphates or when analyses of concrete reveal high sulphate content is not evidence of damage and/or loss of the durability in concrete structures. However, loss of strength and/or visible deterioration accompanied by high sulphate contents would be evidence of sulphate attack [5]. Sulfate attack in concrete can manifest in the form of [6] (i) expansion and cracking or (ii) through a progressive decrease in the strength and loss of mass due to loss of cohesiveness of the cement hydration products. A particular structure will follow the deterioration process described by (i) or (ii) depending on the associated cation of the sulfate ions, its concentration and the composition of the cement paste. When concrete cracks, its durability suffers a detriment because the material is more vulnerable to external attacks of different types.

In general, whether or not concrete has undergone sulphate attack can be established by determining the change in the compressive strength since the time of placing the concrete [1]. The principal reactions of sulphates with hydrated cement paste can be described as follows. (i) Calcium sulphate ($CaSO_4$) reacts: calcium sulphate reacts with C_3A to form ettringite ($C_6A\bar{S}_3H_{32}$); where following the cement chemistry the symbols C, A, $\bar{S}$ and H stand for CaO, Al_2O_3 and SO_3, respectively. Ettringite can cause expansion, cracking, and deterioration of concrete. In addition, calcium sulphate also reacts with sodium and potassium hydroxides. (ii) Magnesium sulphate ($MgSO_4$) reacts: The magnesium sulphate attack is more severe on concrete than sodium or calcium attack. Magnesium sulphate reacts with all products of hydration of cement. The conversion of $Ca(OH)_2$ to gypsum is accompanied by the simultaneous formation of magnesium hydroxide which reduces the alkalinity of the system affecting the stability of the calcium silicate hydrate (C-S-H); when the fact that the term is hyphenated signifies that it is not a well-defined chemical compound [6]. The C-S-H gel is responsible for the strength of cement concrete [7]. (iii) Sodium sulphate (Na_2SO_4): sodium sulphate reacts with portlandite $Ca(OH)_2$, monosulphate and unreacted C_3A to form calcium sulphate (gypsum) and ettringite. In this sense, Eqs.(1)-(4) [8] can explain the expansive products formed after the accelerated or normal attack. Eqs.(1)-(4) were written using the cement chemistry: symbols C, A, S, $\bar{S}$ and H stand for CaO, Al_2O_3, SiO_2, SO_3 and H_2O, respectively.

$$CH + Na_2SO_4 + 2H_2O \rightarrow C\bar{S}H_2 + 2NaOH \quad (1)$$

$$C - S - H + SO_4^{2-} + H_2O \rightarrow C\bar{S}H_2 \quad (2)$$

$$C_4A\bar{S}H_{12} + 2C\bar{S}H_2 + 16H \rightarrow C_6A\bar{S}_3H_{32} \quad (3)$$

$$C_3A + 3C\bar{S}H_2 + 26H \rightarrow C_6A\bar{S}_3H_{32} \quad (4)$$

Based on the numerous cases of premature failure and costly rehabilitation of concrete structures exposed to diverse sulphate environments there have been several laboratory and field investigations related to this topic. For example Bassuoni and

Nehdi [9] studied the durability of a wide range of self-compacting concretes (SCC) to sulfate attack taken into account other concomitant damage mechanics such as environmental conditions and flexural loading. The results revealed the coexistence of complex deterioration processes in SCC under the combined exposure. Chu and Chen [10] presented a theoretical and experimental study on the attenuation of the ultrasonic expansion wave in concrete suffering sulphate attack. The results showed that the magnitude of the attenuation coefficient of concrete increased with time, reflecting damage evolution in the material caused by sulphate attack. Gao *et al*.[11] investigated the damage process of concrete exposed to sulphate attack under flexural loading and drying-wetting cycles. Their results indicated that compared with the single damage process of sulphate attack, flexural loading and drying-wetting cycles can both accelerate the damage process of concrete subjected to sulphate attack. Ouyang *et al*.[12] studied the damage degree through the variation of surface hardness of concrete under sulfate attack. Based on the experimental results, a new method was suggested to express the damage degree.

Sahmaran *et al*. [13] studied the effect of ordinary Portland cement (OPC), sulfate resistant cement (SRPC), and blended cements with different proportions of natural pozzolan and Class F fly ash subject to different exposure regimes: (i) curing in lime-saturated water, (ii) exposure to 5% Na_2SO_4, and (iii) cyclic exposure to 5% Na_2SO_4 solution at room temperature in which the cycles consisted of wetting-drying and heating-cooling. The sulfate resistance of cements was evaluated by measuring the reduction in compressive strength and length change of mortar specimens. The results showed that the performance of blended cements under sodium sulfate at room temperature was better than that of SRPC when the length change was considered. However, for sulfate attack and cycles of wetting-drying and heating-cooling, SRPC was found to perform better than blended cements when the compressive strength losses were considered. Finally, a recent study carried out by Niu *et al*. [14] they investigated the damage process and failure mechanism of shotcrete under the combined actions of sulfate attack and drying-wetting cycle. The results indicated that localization and directivity of defects would lead to the localized distribution of expansive stress. Hence, the crack in defect region developed significantly faster and was the key factor that limited the durability under sulfate attack.

The present paper is only concerned with external sulphate attack both by using immersion tests and wetting-drying cycles. Looking for more realistic conditions the durability and mechanical tests were carried out on concrete samples instead of neat cement paste or mortar specimens usually employed in cementitious materials. Also, wetting-drying cycles have been implemented in the present work in order to reproduce environmental exposure conditions which usually accompany sulphate attack in field structures. Furthermore, a high sodium sulphate concentration which easily classifies as very severe when following some technical standard has been used to accelerate the deleterious effects on concrete samples. In comparison to the typical full-immersion tests, the present study investigates the durability of concrete samples taking into account physical (cyclic environmental conditions) and structural (compression tests) effects.

2. EXPERIMENTAL DETAILS

2.1 Materials

The fine aggregate was natural siliceous sand with a fineness modulus of 2.1, a saturated surface dry specific gravity of 2.7 and water absorption of 1.4%. Crushed stone with a maximum nominal size of 19 mm, a saturated surface dry specific gravity of 2.6 and water absorption of 1.3% was also used. The source of the aggregates was maintained the same for all the mixes in order to do not disturb the statistical and/or ultrasonic analyses.

2.2 Casting process of concrete samples

Constituent materials were mixed in a mechanical mixer in accordance to ASTM C192 [15]. The concrete mixes consisted of 400 kg/m^3 of ordinary Portland cement conforms to ASTM C1157 [16] with a water-to-cement ratio of 0.5. The total mixing time was fixed at 5 min. The fresh concrete was poured into 100 mm of diameter and 200 mm in height standard cylinders [17] for testing procedures. The formwork removal occurred 24 h after casting. The samples were cured in limewater at 23-25 °C and 100% relative humidity until failure (see Section 2.4 for the age of testing). The proportions (percent by mass) used in the mix design consisted of 17.0 cement, 8.5 water, 44.0 coarse and 30.5 fine aggregate.

2.3 Process of the sulphate attack

To evaluate the durability of the samples to sulphate attack, several tests were carried out on concrete specimens immersed in a Na_2SO_4 solution. Since dried salts do not react with concrete, it is the concentration of sulphates in water in contact with concrete that is relevant [1], therefore the solution used in this work contains a very high sulphate concentration of 160,000 ppm (16% of sodium sulphate). The temperature of the solution was maintained at around 21±2 °C. The solution was renewed each two weeks, and the pH (8.0-10.0) was controlled at regular intervals of 5 days. A total of 120 wetting-drying cycles were implemented in the present work to try to reproduce typical environmental sulphate exposure conditions. Each day of testing was divided in cycles started in cycle number 0 and finishing in the 120 cycle number. The trial was conducted according to ASTM C1012 standards [18].

Each cycle consisted in wetting, drying and cooling. This combination tries to replicate field conditions for concrete samples in sulphate-rich environments under climatic changes (wetting/drying). During the wetting cycle the experimental samples were immersed into the sulphate solution for 2 hours. After that the specimens were dried at the surface by mean of a towel to avoid water leakage inside the oven. Then the specimens were left to dry in the oven at 105 ± 5 °C for 9 hours. The cooling period started when the specimens were left inside the oven (turned off) for 5 minutes before samples were moved in front to electric fans. This process was developed carefully avoiding suddenly temperature changes and therefore crack formation. A cooling curve was registered for 45 minutes which permitted to control the temperature variations between the oven process and the cooling condition. The cooling curve was monitored by mean of a contact thermometer Fluke 54-II with two K-type thermocouples. Two temperature points were simultaneously registered (1) referred as T1 located near the top/bottom of the specimen and (2) called T2 in the middle region of the specimen (Fig. 1). The described accelerated attack was conducted as soon as the standard curing period of 28 days was completed. Before exposure, the initial physic-mechanical properties of the intact specimens were measured (cycle 0).

Figure 1. Accelerated attack on concrete samples: showing the temperature data acquisition.

2.4 Physical and mechanical tests

Twenty-five concrete samples were prepared three of them were used as control samples and the remaining twenty-two specimens were subjected to accelerated sulphate attack. The specimens´ distribution related to each type of physical or mechanical test is as follows: four samples for volume and weight change were used, those same samples were used also for UPV measurements and eighteen samples for compression tests. In addition, UPV measurements were registered from the 18 specimens before the compression tests. The destructive compression tests were carried out following ASTM C39 [19] procedure at specific ages (each 15 cycles). The UPV, volume and mass change are nondestructive tests also conducted each 15 cycles started in cycle 0. All the tests were developed after each cycle has been finished, that is, after the cooling period. The accelerated attack started in cycle 0 at the concrete maturity of 28 days, and then every 15 cycles were carried out the tests which consisted of: (1) change of volume, (2) mass change, (3) XRD, (4) compression tests, and (5) UPV measurements. In table 1 is included a resume of all tests carried out on the experimental samples. The volume change tests were carried out using a digital caliper (United Precision Machine Inc.) with high precision (1/100 mm) and the readings were developed on the basis of a mold carefully designed to improve the readings. The mass change tests were carried out using a digital balance (± 1.0 g); also these tests were replicated three times to avoid lecture errors. For the XRD tests the powder (passing sieve N° 40) came from the experimental samples failed in the compression tests. Compression tests were developed using an

Amsler universal testing machine (400 kN in capacity). The UPV measurements were developed using Model Portland cement 1006 Pundit Plus by CNS Farnell Ltda equipped with 54 kHz frequency transducers.

Table 1. Test carried out in experimental samples.

Description	*Number of specimens*	*Test*
No attack	3	Compressive strength, UPV and XRD (5 gr)
Sulphate attack	22	Volume and mass changes (4 samples) Compressive strength (18 samples) UPV (all samples) XRD (5 gr)

An acrylic mold (Fig. 2a-2b) was required during the UPV measurements to guarantee the perfect linearity from side to side of the signal because the direct transmission method was employed. Finally, the UPV tests followed the ASTM C597 [20] recommendations.

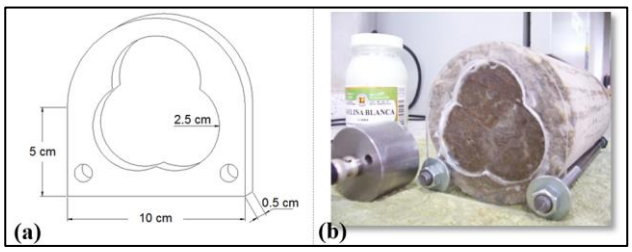

Figure 2. Experimental procedures: (a) UPV mold and (b) UPV setup.

3. RESULTS AND DISCUSSION

3.1 Cooling curve, visual inspection, X-ray diffraction, volume and mass changes

Fig. 3 shows the results of temperature change as registered by the cooling curve when the samples were moved from the oven at 105 ± 5 °C toward room temperature (20-23 °C). As explained earlier the cooling period starts when the oven is turn off, but the cooling curve starts 5 min later when the experimental samples are put in front of fans for approximately 45 min. The results in Fig.3 showed that the samples for the first 15 min of cooling exhibited the highest temperature change. After 14 min of cooling the highest change in temperature is registered in the middle region of the specimen (called T2) with $\Delta T \approx 35$ °C which corresponds with a cooling rate of 0.058 °C/s. The principal objective of the cooling curve consists in monitoring the crack formation which could be induced for drastic temperature changes (thermal cracking). In this sense, following technical literature [21,22] damage to concrete attributable to dehydration of cement hydrates can take place within the concrete at temperatures a little above 100 °C and/or cooling rates above 0.167 °C/s. Therefore it can be seen that neither the oven process nor the cooling rate reached critical values during the heating and/or cooling stages. From Fig. 3 the oven process reached 78 °C as registered in the moment of initial cooling curve monitoring and the cooling rate was almost three times lower than the critical value of 0.167 °C/s. With regard to the high temperature of 105 °C, it is important to take into account that following specialized literature [23, 24] the C-S-H is not strongly disturbed at temperature under 180 °C, being commonly accepted a temperature of 300 °C as the critical limit to induce strongly effects by loss of interlayer and chemically combine water from the C-S-H [6, 25]; whereas at the range of 100 – 200 °C is when the evaporation of free moisture is expected in concrete samples [24, 26]. Specifically until a temperature of 105 °C the paste suffers dehydration but at higher temperatures the aggregate can suffer some expansion effects which could predominate over the volume change of the cement paste and disturb the results [23].

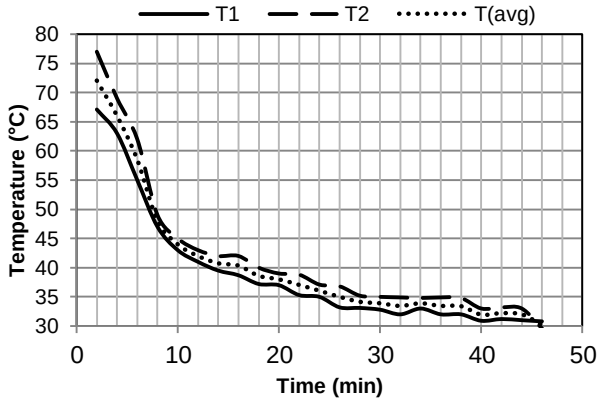

Figure 3. Typical cooling curve: (T1) top/bottom thermocouple and (T2) thermocouple in the middle of the specimen.

During the initial cycles all specimens showed negligible surface damage on the surface. On the other hand, by the end of the exposure, the specimens exhibited marked surface damage which was reflected in small-crack formation (Fig. 4a), scaling (Fig. 4b) and localized expansion (Fig. 4c). Unlike the case of the reference full-immersion in lime water (control specimens), the specimens exposed to both sodium sulphate attack and wetting-drying cycles showed significant surface effects as a result of salt crystallization as confirmed later using XRD analysis. Scaling formation (Fig.4b) is due to leaching of cement materials induced by gypsum formation. The presence of localized expansions (Fig.4c) suggests that expansive products are not formed in a uniform way inside the concrete specimens. The crack formation after 60 cycles is a consequence of formation of expansive products which generate internal tensions that easily exceed the concrete tensile strength and produce cracking (Fig.4c).

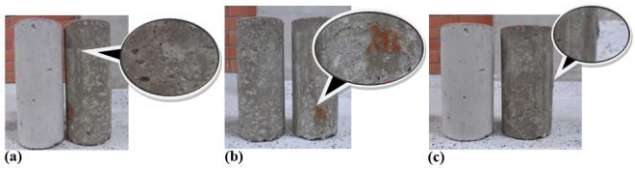

Figure 4. Visual features without attack (left specimen) and immersed in Na_2SO_4 (right specimen): (a) cycle number 90, (b) cycle number 105 and (c) cycle number 120.

With comparison purposes the ASTM C1012 [18] allows an expansion of up to 0.10% for smaller mortar bars and w/cm ratio of 0.485, after 12 months of immersion in a 5% sodium sulphate solution. In the present research, Fig. 5 revealed 0.103% of expansion in diameter after 75 cycles whereas the expansion in length was of 0.117% after 60 cycles of sulphate attack and wetting-drying cycles. In this sense, the present research with the conditions experimented here after 60 cycles suffered a similar attack to those after 12 month of immersion in 5% sulphate solution when following the ASTM standard procedure. At the end of the present experiments all expansion values exceeded 0.10%, that is, the length (0.207%) and diameter (0.218%) expansions were twice the critical value found in the ASTM C1012 reference standard. Therefore, from Eqs.(1)-(4) the symbol $C\bar{S}H_2$ stands for gypsum and from Eqs.(1) and (2) it can be seen that $C\bar{S}H_2$ precipitates from the reaction between $Ca(OH)_2$ and/or calcium silicate hydrates (C-S-H), and the external sulphates. Eq. (2) is showing that the mechanical properties of the concrete samples can be seriously altered because decalcification of C-S-H in a very high sulphate concentration such as in the present work. On the other hand, Eqs. (3) and (4) are showing the formation of ettringite ($C_6A\bar{S}_3H_{32}$) from monosulfoaluminate (Eq. 3) and unreacted tricalcium aluminate (C_3A) grains (Eq. 4).

Fig. 5 shows the results from length, diameter and absorption changes after sulphate exposure. Up to 15 and 30 cycles of accelerated damage, specimens had a tendency to loss diameter and length, respectively. It is promoted by water evaporation inside the specimens. Thereafter, experimental samples experienced an abrupt increase in length up to cycle number 105 and a more moderated but constantly increase in diameter up to cycle number 120. The average absorption of solution each 15 cycles is also shown in Fig. 5. It can be seen that the absorption profile changes through time conforms the attack proceeds. From cycle 0 to 15 the samples experienced the highest change in absorption, this is because the experimental samples come from the oven process and all the internal spaces available to absorb water are empty to do so. Then, during the cycles number 15 and 30 the experiments showed the higher absorption capacities. Thereafter, the process exhibited a decreasing tendency and finally after cycle number 105 the process tended to be stable with approximately 25 g (Fig. 5). The decreasing tendency after 15 cycles suggests crystallization of sodium sulphate with the concomitant reduction in available space into the solid concrete microstructure. The absorption process can continue in a dynamic form because the sulphate attack induces crack formation, therefore new space will be available to be filled with additional crystallization products from the sodium sulphate solution. Despite the extremely high concentration of the sulphate solution in the present work (160,000 ppm of SO_4^{2-}) and the 120 drying-wetting cycles, the specimens did not show any evidence of softening, spalling or macro-cracks on the surface at the end of the exposure period. However, even though the expansions in length and diameter were higher than 0.10% after 60 cycles, the present concrete mixtures cannot be classified as deficient

sulphate resistant, based for example on the full-immersion test followed by the ASTM C1012 [18], because the expansions in the present work were induced by both immersion test and wetting-drying cycles.

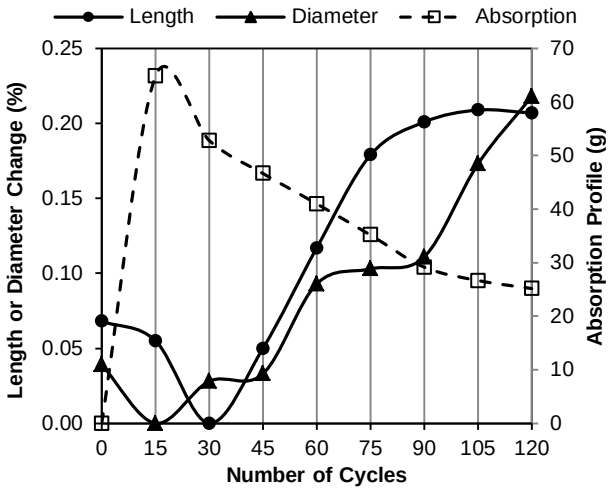

Figure 5. Average of length, diameter and volume changes in the samples after sodium sulphate exposure.

Fig. 6 revealed that in general the mass and volume change followed different patterns. The mass increased from cycle number 15 up to cycle number 60. Thereafter the tendency was toward a reduction as registered at the end of the experimental program (cycle number 120). The increase in mass content is attributable to crystallization of salts from the sulphate attack into the porous structure [21]. Despite the observed surface scaling (Fig. 4b), the experimental samples had slight mass gain over their respective time of exposure. For example, in the last cycle of the experiments the mass content was about 0.05 kg higher than the initial value. The decrease in mass after 60 cycles is related to the scaling and/or leaching processes carried out by the accelerated attack. In general no severe mass loss was observed, the average mass loss through the experimental program was of 1.26% (regards the initial value) and the maximum value was of approximately 1.8% in the cycle number 60 (Fig. 6). On the other hand, the volume change exhibited an initial decrease from cycle number 0 to cycle number 30; thereafter an increasing pattern up to the end of the experimental program (120 cycles) was followed.

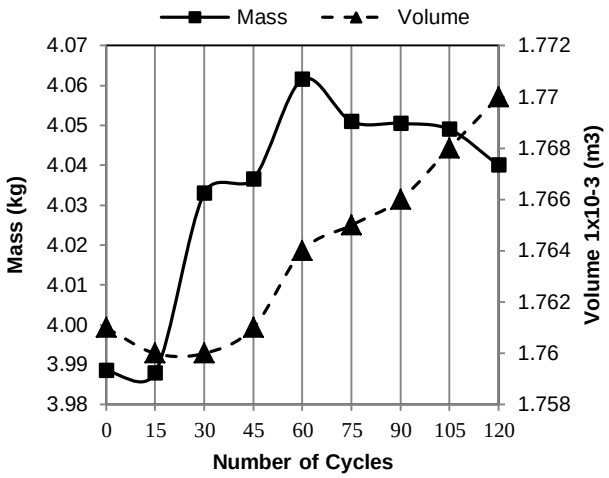

Figure 6. Average of volume and mass in the samples after sodium sulphate exposure.

As explained earlier, the initial decrease in volume is related to the dehydration of the concrete samples induced by loss of evaporable water. The increase in volume is also related to crystallization of salts from the sulphate attack into the porous structure as will be revealed later by XRD analysis. That is, following to Campbell-Allen and Roper [27] one of the most typical forms of deterioration of Portland cement concrete exposed to sulphates may be ascribed to the conversion of CH derived from cement hydration reactions to calcium sulphate (Eq. 5), and the crystallization of this compound with resulting expansion and disruption.

$$CH + SO_4^{2-} + 2H_2O \rightarrow CaSO_4 \cdot 2H_2O + 2OH^- \quad (5)$$

Table 2 shows the XRD analysis carried out through time of exposure of the experimental concrete samples. In Table 2 the source of the crystalline phase is described, that is, the source could be from either the cement, aggregates, cement hydration or from the reaction products coming from the accelerated sulphate attack. As stated earlier (Table 2 and Eqs. 1, 2 and 5), the increase in volume is attributable to formation of expansive products such as gypsum ($CaSO_4 \cdot (H_2O)_2$ or $C\bar{S}H_2$) after 75 cycles of exposure and/or ettringite which was constantly formed through the experiments: $Ca_6Al_2(SO_4)_3(OH)_{12}(H_2O)_{26}$ following the nomenclature from Table 2 or $C_6A\bar{S}_3H_{32}$ following the cement chemistry notation (Eqs. 3 and 4). The initial gypsum amount linked to cycle number 0 is related to the cement hydration process, therefore

cannot be considered as deleterious in the present context. From the XRD analysis it is possible to conclude that neither thaumasite nor $Na_2SO_4 \cdot 10H_2O$ (mirabilite) was formed. Since the sodium sulfate belongs to the type of hydratable salts, at 20 °C and relative humidity (RH) ≥ 72% or 32 °C and RH ≥ 81% the Na_2SO_4 (thenardeite) can convert into its hydrated form $Na_2SO_4 \cdot 10H_2O$. This change is accompanied with important volumetric expansions as a result of large differences in the densities [6]; whereas progressive replacement of C-S-H with thaumasite usually produces a pulpy mass with non-binding characteristics [9]. Therefore the XRD results can explain the moderate expansion observed at the end of the test (cycle number 120 with approximately 0.21% of expansion in length and diameter). In addition, the XRD results explain the fact that experimental samples did not suffer the softening processes even though the extremely high sulphate content and the wetting-drying cycles. Finally, the XRD analysis also shown the formation of classical products of sulphate attack such as $Ca_{1.31}Na_{4.32}(OH)_{0.94}(SO_4)_3$, $Ca_3Al_2(O_4H_4)_3$ and Na_2SO_4.

Table 2. XRD results from experimental concrete samples under sulphate attack

Source[a]	*Crystalline phase*	*Number of Cycles*								
		0	15	30	45	60	75	90	105	120
A/C	$Na(AlSi_3O_8)$									
A/C	$(Na,Ca)Al(Si,Al)_3O_8$									
A/C	$CaCO_3$									
A/C	$Al_2Si_2O_5(OH)_4$									
A/C	$(Mg,Fe)_6(Si,Al)_4O_{10}(OH)_8$									
A/C	SiO_2									
A/C	Ca_2SiO_4									
A/C	$KAl_2(Si,Al)_4O_{10}(OH)_2$									
A/C	TiO_2									
HC	$Ca(OH)_2$									
HC	$Ca_4(Si_6O_{15})(OH)_2(H_2O)_5$									
SA	$Ca_{1.31}Na_{4.32}(OH)_{0.94}(SO_4)_3$									
SA	$Ca_6Al_2(SO_4)_3(OH)_{12}(H_2O)_{26}$									
SA	$Ca_3Al_2(O_4H_4)_3$									
SA	Na_2SO_4									
SA	$Ca(SO_4)(H_2O)_2$									

[a] The symbols A/C, HC and SA stand for aggregate and/or cement, cement hydration and sulphate attack, respectively.

3.2 Relationship between density and compressive strength versus UPV measurements

Fig. 7 shows the relationship between compressive strength (Sc) expressed in MPa and UPV values (m/s) both as a function of the cycle number. Table 3 summarizes the analysis of variance (ANOVA) results carried out for compressive and UPV values following the so-called fixed-effects model. By using this statistical procedure the mean values of each one of the variables analyzed (Sc and UPV) are supposed to be equal through the experimental cycles, this is called the null hypothesis. If the null hypothesis is true, the ratio expresses by the *F*-test (F_o) follows a Fischer distribution and the *P*-value is supposed to be greater than 0.05 (5% of significance). Since the *P*-values of Table 3 are both considerable smaller than 0.05 there is strong evidence to conclude that the cycle number has a statistical effect on compressive and UPV measurements (5% of significance).

Table 3 shows that cycle number has an effect on both compressive strength and UPV values. However, the ANOVA does not explain which cycle

numbers result in different compressive or UPV mean values, therefore the Fisher Least Significant Difference (LSD) method was used to answer this question at 5% level. By using LSD the null hypotheses to be tested is (Eq. 6):

$$H_o: \mu_i = \mu_j \quad \text{for all} \quad i \neq j \qquad (6)$$

Assuming a two-sided alternative, the pair of means μ_i and μ_j is declared statistical significantly different if the relation in Eq. 7 is possible.

$$|\bar{y}_{i.} - \bar{y}_{j.}| > t_{\propto \frac{1}{2}, N-a} \sqrt{MS_E \left(\frac{1}{n_i} + \frac{1}{n_j}\right)} = LSD \qquad (7)$$

The term *N-a* refers to the degrees-of-freedom, n_i and n_j are the sample sizes and MS_E is the error mean square. Therefore, the procedure consisting in compares the observed difference between each pair of averages to the corresponding *LSD*. If Eq. 6 is satisfied then, the conclusion is that population means differ [28]. The results for compressive strength and UPV values are shown in Table 4.

From Fig. 7 it is noted that UPV measurements exhibited a pronounced nonlinear behavior through the sulphate attack and wetting-drying cycles reaching a peak value in the cycle number 60. The compressive strength behavior is also nonlinear but its curvature is lesser pronounced than the UPV behavior through the experimental program.

Table 3. ANOVA results for compression and UPV measurements.

Variable Analyzed	*Source of Variation*	*Sum of Squares*	*Degrees of Freedom*	*Mean Square*	F_o	*P-value*
Sc (MPa)	Between cycles	95.77	8	11.97	24.81	0.0000
	Inside cycles	4.342	9	0.48		
UPV (m/s)	Between cycles	8.17E4	8	1.02E4	13.88	0.0003
	Inside cycles	6627.0	9	736.40		

Table 4. Fisher Least Significant Difference for compressive and UPV values.

CONTRAST:	SIGNIFICANT		CONTRAST:	SIGNIFICANT	
Cycles	Sc (MPa)	UPV (m/s)	Cycles	Sc (MPa)	UPV (m/s)
120 – 00	No	No	90 – 45	No	No
120 – 15	No	No	90 – 60	Yes	No
120 – 30	Yes	Yes	90 – 75	Yes	No
120 – 45	Yes	Yes	75 – 00	Yes	Yes
120 – 60	Yes	Yes	75 – 15	Yes	Yes
120 – 75	Yes	Yes	75 – 30	Yes	Yes
120 – 90	Yes	Yes	75 – 45	No	No
120 – 105	Yes	Yes	75 – 60	No	No
105 – 00	Yes	Yes	60 – 00	Yes	Yes
105 – 15	Yes	Yes	60 – 15	Yes	Yes
105 – 30	No	No	60 – 30	Yes	Yes
105 – 45	Yes	No	60 – 45	No	No
105 – 60	Yes	No	45 – 00	Yes	Yes
105 – 75	Yes	No	45 – 15	Yes	Yes
105 – 90	No	No	45 – 30	Yes	Yes
90 – 00	Yes	Yes	30 – 00	Yes	Yes
90 – 15	Yes	Yes	30 – 15	No	No
90 – 30	Yes	Yes	15 – 00	No	Yes

The compressive strength pattern agreed with the UPV measurements and the compression peak coincided with that of the UPV maximum value, that is, in the cycle number 60. However, it is important to take into account that peak value at cycle 60 for Sc and UPV measurements is not statistically different from the peak values found at 45 and 75 cycles following the *LSD* methodology at 5% of significance (Table 4). Nevertheless, from laboratory tests a nonlinear regression analysis between the average of four UPVs measurements and two compression values were performed obtaining a correlation coefficient equal to 0.9874 by using an exponential model (Eq. 8) which was the best fitted model. The concave pattern (Fig.7) registered in both compression values and UPV measurements could be explained because the presence of voids in concrete decreases its compressive strength [29] and therefore the UPV values. When the water evaporates during dry process, salt is deposited on the surface of the concrete; in consequence, concrete is damaged. It is, therefore, logical to expect leaching of hydration products and/or crack formation induced by sulphate attack to cause a reduction in the compressive strength and therefore in the UPV measurements. Thus, it is reasonable to conclude that the material has suffered damage when a reduction in the mechanical properties through time is observed such as after 60 accelerated cycles in Fig. 7.

$$Sc(UPV) = Exp(-0.7129 + 0.001084 * UPV) \quad (8)$$

There was a general increase in mechanical and physical properties up to 60 cycles due to continuous hydration of the matrix and filling of voids with reaction products both from cement hydration and from the sulphate attack. It is corroborate from the pattern in Figs.5 and 6 where the absorption of the solution and mass content were increased at the beginning of the experimental program (up to 15 cycles for absorption and up to 60 cycles for mass). It is noteworthy to note that mass change, compressive strength and UPV measurements coincided in the peak value at cycle number 60.

Thereafter, the leaching and scaling processes induced loss of mass and the mechanical properties of the concrete samples decreased. In a similar fashion the relationship between two density values (ρ) expressed as kg/m^3 and UPV measurements as a function of the number of cycles is depicted in Fig.8.

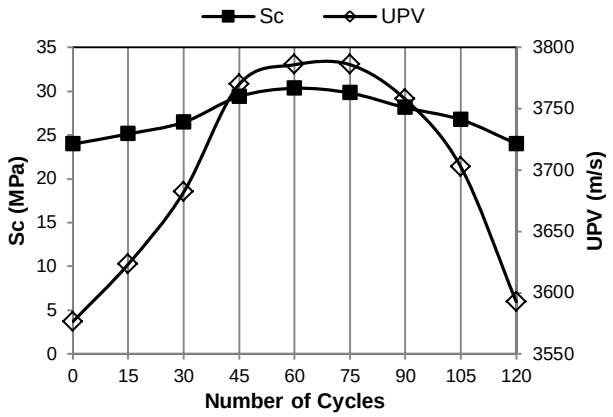

Figure 7. UPV and compressive strength after sodium sulphate exposure.

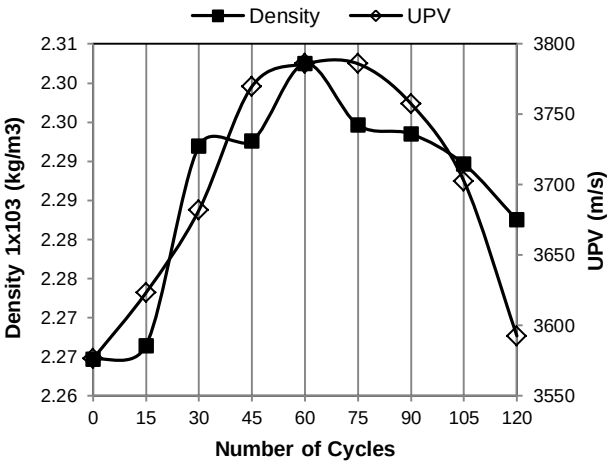

Figure 8. UPV and density changes after sodium sulphate exposure.

The pattern followed by the density is the same as that by the mass change in Fig.6 and UPV values in Fig. 7. Also, the peak value of density is found at the cycle number 60. This trend shows that the most important variable related to the change in density was the mass change rather than the volume change. From laboratory tests a regression analysis between the average of four UPVs and two density values were performed obtaining a correlation coefficient equal to 0.9291 and *P*-value of 0.0027 by using a linear model (Eq. 9) which was the best fitted model. Since the *P*-value was smaller than 0.05, the statistical relationship is considered to be strong (at

least at 5% level). Comparatively, the behavior captured in Figs. 7 and 8 agreed with results from Fig.5 where the critical limit of 0.10% from Ref. [18] was reached after 60 and 75 cycles for expansion in length and diameter, respectively. These results provide physical evidence to show that the UPV technique is useful to detect microstructural changes from accelerated sulphate attack on concrete samples. The physical evidence is based on the correlation between the critical expansion and the decrease in the mechanical (Sc) and physical (ρ) properties in concrete specimens.

$$\rho(UPV) = 1789 + 0.1345 * UPV \quad (9)$$

4. CONCLUSIONS

This paper has presented an experimental study on concrete specimens under both accelerated sulphate attack and wetting-drying cycles. Mathematical relationships between density and UPV as well as compressive strength and UPV measurements have been derived. In addition, visual inspection and XRD analyses were carried out. From the present study the following conclusions can be drawn.

The cooling curve results showed that the samples for the first 15 min of cooling exhibited the highest temperature change ($\Delta T \approx 35$ °C) registered in the middle region of the specimen. The temperature change corresponds with a cooling rate of 0.058 °C/s. Since damage to concrete attributable to dehydration of cement hydrates can take place above 100 °C and/or cooling rates above 0.167 °C/s. Therefore it could be concluded that neither the oven process nor the cooling rate reached critical values during the heating and/or cooling stages. Consequently all the results in the present work were attributable solely to the accelerated sulphate and wetting-drying cycles without additional damage induced by thermal cracking.

Unlike the case of the reference full-immersion exposure in lime water at 20-23 °C, the specimens exposed to both sodium sulphate attack and wetting-drying cycles showed significant surface effects as a result of salt crystallization as confirmed by XRD analysis. Cracking, scaling and expansions after 60 cycles are a consequence of formation of expansive products which generate internal tensions that easily exceeded the concrete tensile strength.

After 60 cycles of sulphate attack and wetting-drying cycles there was 0.103% of expansion in diameter; whereas after 75 cycles the expansion in length was of 0.117%. Comparatively, the ASTM C1012 allows an expansion up to 0.10% for smaller mortar bars at w/cm ratio of 0.485 after 12 months of immersion in a 5% sodium sulphate solution. Therefore, it can be concluded that experimental conditions in the present research after 60 cycles suffered a similar attack to those after 12 month of full-immersion following the ASTM standard procedure. Also, at the end of the present experiments after 120 cycles, all expansion values exceeded 0.10%. The length and diameter expansions were in average twice the critical value found in the ASTM C1012 reference standard.

The UPV measurements and compressive strength values exhibited a pronounced nonlinear behavior through the experiments reaching a peak value in the cycle number 60. The compressive strength pattern agreed with the UPV and the compression peak coincided with the UPV maximum value in cycle number 60 (which was statistically similar to cycle's number 45 and 75 following the Fischer´s LSD procedure at 5% of significance). A nonlinear regression analysis between the UPV measurements and compression values obtained a correlation coefficient equal to 0.9874 by using an exponential model, which was the best fitted model.

A regression analysis between UPVs and density values (mass and volume change) were performed obtaining a correlation coefficient equal to 0.9291 and *P*-value of 0.0027 by using a linear model which was the best fitted model. The behavior obtained from laboratory tests between UPV and density values agreed with results from expansion in length and diameter. The critical limit of 0.10% following the ASTM C1012 was reached after 60 and 75 cycles for expansion in length and diameter, respectively. These results provide physical evidence to show that the UPV technique is useful to detect microstructural changes in physical and mechanical properties from accelerated sulphate attack on concrete samples. Finally, no severe mass loss was observed and in general the mass and volume followed different patterns as explained in more detail in the document.

5. ACKNOWLEDGEMENT

The authors gratefully acknowledge the technical support of this research to GIMAT and INME

research groups which are part of the Departments of Metallurgy and Materials Science and Civil Engineering, respectively; both at the Universidad Industrial de Santander, Bucaramanga, Colombia. Also, the authors would like to express their sincere thanks to Engineers R.M. Santamaría and G.A. Quiros for their assistance throughout the experimental part of this study.

6. REFERENCES

[1]. Neville A.M, Concrete: Neville´s insights and Issues, London: Thomas Telford Ltd, 2006, pp. 321.

[2]. Nehdi M.L., Suleiman A.R., Soliman A.M., Investigation of concrete exposed to dual sulfate attack. Cement and Concrete Research 64, 2014, p. 42-53.

[3]. Liu Z., Deng D., De Schutter G., Does concrete suffer sulfate salt weathering?. Construction and Building Materials 66, 2014, p. 692-701.

[4]. Norma ACI Committee web letter: 201.2R, Phsycial salt attack, chapter 8, Farmintong, Hills, Mich, United States. American Concrete Institute, 2010.

[5]. Neville A., The confused world of sulfate attack on concrete. Cement and Concrete research 34, 2004, p. 1275-1296.

[6]. Mehta P.K, Monteiro P.J.M. Concrete-microstructure, Properties and Materials. 3rd ed. New York (USA): McGraw-Hill, 2003.

[7]. Caldarone M.A., High-Strength Concrete - A Practical Guide, 1st ed., Taylor& Francis, New York, USA, 2009.

[8]. Idiart A.E., López C.M., Carol I., Chemo-mechanical analysis of concrete cracking and degradation due to external sulfate attack: A meso-scale model. Cement and Concrete Composites 33, 2011, p. 411-423.

[9]. Bassuoni M.T., Nehdi M.L., Durability of self-consolidating concrete to sulfate attack under combined cyclic environments and flexural loading. Cement and Concrete Research 39, 2009, p. 206-226.

[10]. Chu H-Y, Chen J.-K., Evolution of viscosity of concrete under sulphate attack. Construction and Building Materials 39, 2013, p. 46-50.

[11]. Gao J., Yu Z., Song L., Wang T., Wei S. Durability of concrete exposed to sulfate attack under flexural loading and drying-wetting cycles. Construction and Building Materials 39, 2013, p. 33-38.

[12]. W.-Y. Ouyang, J.-K. Chen, M.-Q. Jiang. Evolution of surface hardness of concrete under sulfate attack. Construction and Building Materials 53, 2014, p. 419-424.

[13]. Sahmaran M., Erdem T.K., Yaman I.O., Sulfate resistance of plain and blended cements exposed to wetting-drying and heating-cooling environments. Construction and Building Materials 21, 2007, p. 1771-1778.

[14]. Niu D.-t., Wang Y.-d., Ma R., Wang J.-b., Xu S.-h., Experiment study on the failure mechanism of dry –mix shotcrete under the combined actions of sulfate attack and drying-wetting cycles. Construction and Building Materials 81, 2015, p. 74-80.

[15]. Norma ASTM C192, Standard Practice for Making and Curing Concrete Test Specimens in the Laboratory, 100 Barr Harbor Drive, West Conshohocken, PA 19429, United States. American Society for Testing and Materials, 2007.

[16]. Norma ASTM C1157, Standard Performance Specification for Hydraulic Cement, 100 Barr Harbor Drive, West Conshohocken, PA 19429, United States. American Society for Testing and Materials, 2010.

[17]. Norma ASTM C470, Standard Specifications for Molds for Forming Concrete Test Cylinders Vertically, 100 Barr Harbor Drive, West Conshohocken, PA 19429, United States. American Society for Testing and Materials, 2008.

[18]. Norma ASTM C1012. Standard Test Method for Length Change of Hydraulic-Cement Mortars Exposed to a Sulfate Solution, 100 Barr Harbor Drive, West Conshohocken, PA 19429, United States. American Society for Testing and Materials, 2009.

[19]. Norma ASTM C39, Standard Test Method for Compressive Strength of Cylindrical Concrete Specimens, 100 Barr Harbor Drive, West Conshohocken, PA 19429, United States. American Society for Testing and Materials, 2011.

[20]. Norma ASTM C597, Standard Test Method for Pulse Velocity Through Concrete, 100 Barr Harbor Drive, West Conshohocken, PA 19429, United States. American Society for Testing and Materials, 2002.

[21]. Newman J., Choo B.S., Advanced Concrete Technology –Testing and Quality. Butterworth-Heinemann, Oxford OX2 8DP 200 Wheeler Road, Burlington MA 01803, 2004, ISBN 0 7506 5106 7.

[22]. Verkehrsblatt-Sammlung Nr. S1056: ZTV-ING, Teil 5 Tunnelbau, Abschnitt 1 Geschlossene Bauweise, Stand 12/2007.

[23]. Ercolani G.D., Ortega N.F., Señas L., Empleo de Ultrasonidos y Esclerometría en el diagnóstico de estructuras de hormigón afectadas por elevadas temperaturas. Proceedings IV Conferencia Panamericana de END 2007. Buenos Aires (Argentina): Asociación Argentina de Ensayos No Destructivos y Estructurales (AAENDE), 2007, p. 1-10.

[24]. Di Maio A., Ferreyra Hirschi E., Giaccio G., Zerbino R., Hormigones expuestos a altas temperaturas: evaluación de la permeabilidad y otras propiedades físicas. Anales SAM 1999. Buenos Aires (Argentina): Asociación Argentina de Materiales, 1999, p. 204-209.

[25]. Colombo M., Felicetti R., New NDT techniques for the assessment of fire-damaged concrete structures. Fire Safety Journal 42, 2007, p. 461-472.

[26]. Georgali B., Tsakiridis P.E., Microstructure of fire-damaged concrete. A case study. Cement and Concrete Composites 27, 2005, p. 255-259.

[27]. Campbell-Allen D., Roper H. Concrete Structures: Materials, Maintenance and Repair. New York (USA): Longman Scientific & Technical, Wiley, 1991.

[28]. Montgomery D. C. Design and Analysis of Experiments. 5th edition. New York (USA): John Wiley & Sons, Inc., 2001.

[29]. Ashby M.F., Jones D.R. Engineering Materials 1 – An Introduction to Properties, Applications and Design. Third Edition, Butterwoth-Heinemann (Elsevier), Linacre House, Jordan Hill, Oxford, 2005.